



Real-time Imaging of the Electric Conductivity Distribution inside a Rechargeable Battery Cell

Matsuda, Seiju ; Suzuki, Shogo ; Yabumoto, Kai ; Okada, Hideaki ; Mima, Yuki ; Kimura, Noriaki ; Kimura, Kenjiro

(Citation)

Electrochemistry, 89(5):420-426

(Issue Date)

2021-09-05

(Resource Type)

journal article

(Version)

Version of Record

(Rights)

© The Author(s) 2021. Published by ECSJ.

This is an open access article distributed under the terms of the Creative Commons Attribution 4.0 License (CC BY), which permits unrestricted reuse of the work in any medium provided the original work is properly cited.

(URL)

<https://hdl.handle.net/20.500.14094/90008586>



Real-time Imaging of the Electric Conductivity Distribution inside a Rechargeable Battery Cell

Seiju MATSUDA,^{a,§} Shogo SUZUKI,^a Kai YABUMOTO,^a Hideaki OKADA,^a
Yuki MIMA,^{b,c} Noriaki KIMURA,^{b,c} and Kenjiro KIMURA^{a,c,d,*}

^a Graduate School of Science, Kobe University, 1-1 Rokkodai-cho, Nada-ku, Kobe, Hyogo 657-8501, Japan

^b Integral Geometry Science, 1-5-6 Minatojima-minamimachi, Chuo-ku, Kobe, Hyogo 650-0047, Japan

^c New Energy and Industrial Technology Development Organization, 1310 Omiya-cho, Saiwai-ku, Kawasaki, Kanagawa 212-0014, Japan

^d Center for Mathematical and Data Sciences, Kobe University, 1-1 Rokkodai-cho, Nada-ku, Kobe, Hyogo 657-8501, Japan

* Corresponding author: kimura@gold.kobe-u.ac.jp

ABSTRACT

The aim of this study is to observe the spatial inhomogeneity of a rechargeable battery's electric conductivity distribution. Therefore, we have developed a system that uses the measurement results of a minute magnetic field that leaks from the cell to visualize, in real time, the cell's electric conductivity distribution. This system has a magnetic detection capability of 30 pT/Hz^{0.5} (at 1 Hz); it measures the magnetic field distribution in the 240 × 240-mm range. This system has the ability to detect the 500-μA electric current that flows in a rechargeable battery 5 mm away from the sensor module. Because the magnetic signals are detected at the frequency synchronized with the alternating current flowing in the cell, this system is not affected by environmental magnetic field noise. Using this system, we have successfully visualized the short-circuit spot in a cell with significant self-discharge. Furthermore, we observe that the magnetic field distribution changes continually when the short circuit is being generated. The coordinate where the magnetic field distribution changed and the coordinate where metal precipitates were confirmed significant agreement.

© The Author(s) 2021. Published by ECSJ. This is an open access article distributed under the terms of the Creative Commons Attribution 4.0 License (CC BY, <http://creativecommons.org/licenses/by/4.0/>), which permits unrestricted reuse of the work in any medium provided the original work is properly cited. [DOI: 10.5796/electrochemistry.21-00007].



Keywords : Lithium-ion Battery, Electric Conductivity Distribution, Magnetic Field Distribution, Real Time

1. Introduction

Studies regarding the creation of a lithium-ion rechargeable battery with high energy density are conducted worldwide, and the demand for a high-quality battery continues to increase.¹ The spatial inhomogeneity of the reaction on the electrode in the rechargeable battery causes dendritic metal to precipitate on the electrode.^{2–4} It is known that the precipitated metal short circuits between the electrodes lead to thermorunaway.^{5–7} This has been confirmed by studies that have conducted in-situ observations with a laser scanning confocal microscope⁸ and ex-situ observations with a Scanning Electron Microscope (SEM).⁹ To elucidate the dynamic behavior of the moment when a short circuit forms inside a cell, in cases when the internal short circuit and the thermorunaway were caused by nail penetration,^{10–12} researchers have used heat measurement¹³ and an electrochemical impedance measurement.¹⁴ Because the behavior of the battery in a failure status depends on the operating condition and the cell state, the development of a technique to visualize the internal state in detail is necessary. To date, research has reported on observations obtained via simulation^{15,16} and how the use of X-rays changes the behavior of the layered structure of an electrode.^{17,18}

In this study, to non-destructively observe the electric current flowing inside of the rechargeable battery, we focus on the magnetic field that occurs in the surroundings of cell as a result of said current. Because the rechargeable battery is made of non-magnetic materials, such as aluminum and copper, magnetic field that occurs because of the electric current flowing through the electrode leaks out of the cell. Thus, by detecting the magnetic field distribution outside the

rechargeable battery and reconstituting the electric conductivity distribution based on the magnetic field distribution, the electric conductivity inside the rechargeable battery can be visualized non-destructively.


To determine when the internal state changes during the cell operation, such as when the internal short circuit forms, it is essential to monitor with real-time. The system developed in this study comprises a magnetic sensor module that is created by arranging said sensor, which uses a magnetic impedance effect as a detection principle, two-dimensionally in 24 × 24 ch. This magnetic sensor module can acquire the magnetic field distribution in a range of 240 × 240 mm, which is sufficient to measure the entire lithium-ion battery, the size of which has increased in recent years. Furthermore, this system quickly visualizes the electric conductivity distribution in the cell and non-destructively by employing a theory that uses the measured magnetic field data to analytically solve equations regarding the electric current and the static magnetic field in the rechargeable battery. This system is not affected by environmental magnetic field noise because it detects at the frequency of the alternating current flowing through the cell. Therefore, it is possible to take measurements without the need of magnetic shield that is generally used for micromagnetic field measurements. In this paper, we report on our system, which visualizes the electric conductivity distribution inside the rechargeable battery in detail. Additionally, we will report on the result of visualizing the short-circuit point of the single-layer lithium-ion battery, and the result of the state of the short circuit changing between the electrodes due to the electrodeposition of the ions in the electrolytic solution when the electric current is applied.

2. Theory

Based on the magnetic field distribution measured outside of

[§]ECSJ Student Member

^{§§}ECSJ Active Member

S. Matsuda  orcid.org/0000-0002-1637-9022

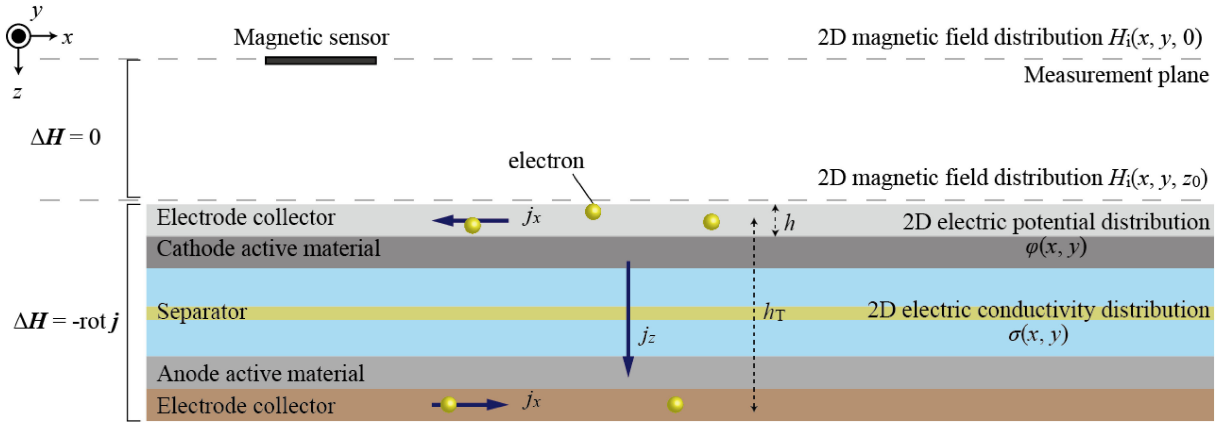


Figure 1. Definition of each variable of the process of reconstituting the electric conductivity distribution in the cell from the magnetic field leaking from the cell in the single-layer rechargeable battery.

the cell, it is necessary to develop a computational algorithm to reconstitute the electric current flow on or between the electrodes. In this study, we used techniques to analytically solve inverse problems regarding basic equations of the electric current in the rechargeable battery and the static magnetic field inside and outside of the rechargeable battery.^{19,20} As shown in Fig. 1, from the magnetic field distribution $H_i(x, y, 0)$ obtained by the measurement, the magnetic field distribution $H_i(x, y, z_0)$ near the storage battery is obtained, and with this as the boundary condition, the potential distribution $\varphi(x, y)$ on the electrode and the two-dimensional electric conductivity distribution $\sigma(x, y)$ in the storage battery is derived.

2.1 Basic equations of the current and the magnetic field in a non-existent space of the current

In free space where there is no current source, the basic equation of the static magnetic field is Laplace's equation like Eq. (1). Δ is Laplace operator. The x -axis and the y -axis are parallel to the electrodes, and the z -axis is the normal direction.

$$\Delta H_i = 0 \quad (i = x, y) \quad (1)$$

Assigning the two-dimensional Fourier transform $f_i(k_x, k_y)$ of the measured magnetic field distribution in Eq. (2) as the boundary conditions, the solution of Eq. (1) is derived by Eq. (3).¹⁹

$$f_i(k_x, k_y) = \int_{-\infty}^{\infty} \int_{-\infty}^{\infty} e^{-ik_x x - ik_y y} H_i(x, y, 0) dx dy \quad (i = x, y) \quad (2)$$

$$H_i(x, y, z_0) = \frac{1}{(2\pi)^2} \iint e^{ik_x x + ik_y y} \{f_i(k_x, k_y) e^{z_0 \sqrt{k_x^2 + k_y^2}}\} dk_x dk_y \quad (3)$$

By substituting the magnetic field distribution $H_i(x, y, 0)$ obtained by the measurement into Eqs. (2), (3), the magnetic field distribution $H_i(x, y, z_0)$ near the battery can be derived.

2.2 Analytical solution for current and magnetic field near the storage battery

The relationship between the magnetic field distribution on the surface of a single-layered lithium-ion battery and the electric conductivity within said battery (shown in Fig. 1) can be derived using Eq. (4). In Eq. (4), h_T is the distance between collectors; h is the thickness of the collector; z_0 is a coordinate of the electrode; σ_0 is the electric conductivity of the collector; $\sigma(x, y)$ is the two-dimensional electric conductivity distribution between the anode collector and the cathode collector in the battery; and $\varphi(x, y)$ is the two-dimensional potential difference distribution on the collector surface. δ is delta function, and δ' is a function obtained by differentiating the delta function in the z direction. The current flowing over the positive and negative electrodes is expressed as

a gradient of φ . Therefore, all of these effects are taken into consideration in the following Poisson's equation with φ as the source term and the magnetic field as the left side.

$$\begin{aligned} \Delta H_x &= h_T^{-1} h \frac{\partial}{\partial y} \{ \sigma(x, y) \varphi(x, y) \} \delta(z - z_0) \\ &\quad - \sigma_0 h \left\{ \frac{\partial}{\partial y} \varphi(x, y) \right\} \delta'(z - z_0) \\ \Delta H_y &= -h_T^{-1} h \frac{\partial}{\partial x} \{ \sigma(x, y) \varphi(x, y) \} \delta(z - z_0) \\ &\quad + \sigma_0 h \left\{ \frac{\partial}{\partial x} \varphi(x, y) \right\} \delta'(z - z_0) \\ \Delta H_z &= \frac{\partial}{\partial x} \left\{ \sigma_0 h \frac{\partial}{\partial y} \varphi(x, y) \delta(z - z_0) \right\} \\ &\quad - \frac{\partial}{\partial y} \left\{ \sigma_0 h \frac{\partial}{\partial x} \varphi(x, y) \delta(z - z_0) \right\} = 0 \\ \frac{\partial^2}{\partial x^2} \varphi + \frac{\partial^2}{\partial y^2} \varphi &= (\sigma_0 h h_T)^{-1} \sigma(x, y) \varphi(x, y) \end{aligned} \quad (4)$$

However, this theory does not define the existence of current input/output points such as tabs. When the tab positions of the positive electrode and the negative electrode, which are the input/output points of the current, are different, they cannot be handled together and it is impossible to describe them with only one variable (φ). This problem can be solved by applying the difference data between the measured data and the magnetic field distribution of cells (reference cells) with the same structure to the theory, as described 3.1. This cancels out the potential at current input/output points and the ends of the electrodes. Further, the z -coordinates of the magnetic field derived from the positive electrode and the magnetic field derived from the negative electrode differ by h_T , but this is small enough that it does not matter.

From Eq. (4), the electric current flowing on the conductor surface does not produce the z -component, H_z , of the magnetic field vector. Furthermore, considering that the electric current flowing between the electrodes flows in the z -axis direction, this electric current also does not produce H_z . Therefore, in a cell, such as a square lithium-ion battery that does not have a curved electrode surface, the magnetic field distribution in the x or y direction is an effective measurement target. As shown in Eq. (2), $Q_x(k_x, k_y, z_0)$ and $Q_y(k_x, k_y, z_0)$ are assumed to be the two-dimensional Fourier transformation images of the x - and y -components, respectively, of the magnetic field, $H_x(x, y, z_0)$, $H_y(x, y, z_0)$.

$$Q_i(k_x, k_y, z_0) = \int_{-\infty}^{\infty} \int_{-\infty}^{\infty} e^{-ik_x x - ik_y y} H_i(x, y, z_0) dx dy \quad (i = x, y) \quad (5)$$

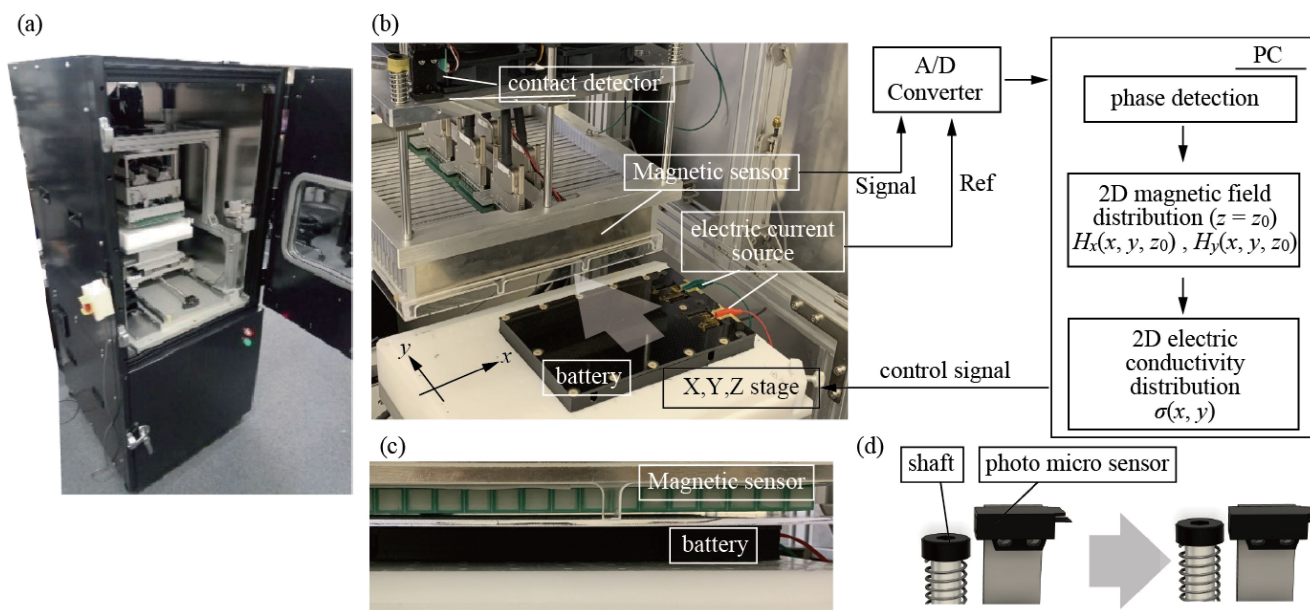


Figure 2. Overview of the electric conductivity distribution inside a battery cell imaging system developed in this study. (a) The entire system and (b) the neighborhood of the cell and the magnetic field detecting component. The rechargeable battery cell is installed on the X, Y, and Z stages with a fixture, and the cell moves directly under the magnetic sensor at the time of the measurement by moving the X and Y stages; (c) the time at which the magnetic field distribution measurement occurred and (d) a component detecting the contact between the magnetic sensor module and the rechargeable battery. Contact between the sensor module and the cell is detected by determining the displacement of the shaft fixed to the sensor module with the photo-microsensor.

Using Eq. (5), $\varphi(x, y)$ can be derived from Eq. (4), as shown in Eq. (6).¹⁹

$$\varphi(x, y) = \frac{1}{(2\pi)^2} \int_{-\infty}^{\infty} \int_{-\infty}^{\infty} \frac{2\{ik_y Q_x(k_x, k_y, z_0) - ik_x Q_y(k_x, k_y, z_0)\}}{h\sigma_0(k_x^2 + k_y^2)(h\sqrt{k_x^2 + k_y^2} - 1)} dk_x dk_y \quad (6)$$

Additionally, the two-dimensional electric conductivity distribution $\sigma(x, y)$ in the battery can be found using Eq. (7).

$$\sigma(x, y) = \frac{h h_T \sigma_0 \left(\frac{\partial^2}{\partial x^2} + \frac{\partial^2}{\partial y^2} \right) \varphi(x, y)}{\varphi(x, y)} \quad (7)$$

The two-dimensional electric conductivity distribution in the rechargeable battery represents the ease of the inflow/outflow of electrons between the cathode and the anode; this includes the cell reaction on the electrode and the movement of ions. Based on this, the electric conductivity distribution in the rechargeable battery can be derived from the magnetic field distribution $H_x(x, y, 0)$, $H_y(x, y, 0)$ obtained by the measurement.

3. Method

The real-time magnetic imaging system developed in this experiment consisted of a control PC, super high-sensitivity magnetic sensor module, contact detection part: X, Y, and Z stages, AC power supply, and A/D converter, as shown in Figs. 2(a) and 2(b). The alternating current that overlapped the DC voltage (and was equal to the electromotive force of the cell) was applied to the cell at the time of the measurement by connecting the cell to an alternating current power supply capable of applying up to 2 A. At this time, the charged state of the rechargeable battery was maintained before and after the measurement, because the electric current applied was the alternating current in a sine wave. When the frequency of the alternating current applied to the cell is high, the magnetic field that leaks out is affected by the shielding due to a

constituent metal of cell. For example, in the case of copper, the depth of the shielding became 2 mm in the magnetic field of 1 kHz. In addition, the effect of dynamic electromagnetic field is not considered in Eqs. (1), (4); therefore, when measuring the rechargeable battery, I set the frequency to less than 10 Hz, which is approximated as a static magnetic field.

The magnetic field leaking from the cell was detected by positioning the X, Y, and Z stages, on which the cell was set up, right under the magnetic sensor module [Fig. 2(c)]. The magnetic sensor module used a magnetic impedance effect²¹ as a principle of magnetic detection. The impedance variation of the magnetic amorphous wire, which was a reception part, was detected and amplified with a preamplifier and assumed to be an output signal. This magnetic sensor, which successfully operated at room temperature, achieved a high magnetism detection capability, i.e., 30 pT/Hz^{0.5} (at 1 Hz) and a maximum magnetic response frequency of 1 kHz. This measurement system was able to detect the magnetic field occurring from the 500-μA electric current that flows inside the rechargeable battery 5 mm away from the sensor module. By mounting this magnetic sensor element in a 24 × 24-ch arrangement with a 10-mm interval on the surface parallel to the electrode of the rechargeable battery, the magnetic field distribution within the measurement range of up to 240 × 240 mm was detected. To observe the cell in detail, an image with the higher number of pixels can be acquired by scanning the X and Y stages to interpolate between the magnetic sensors next to each other, as shown in Fig. 3. At this time, the size of the magnetic reception element was 6 mm, as was the spatial resolution. The minimum time required for measurement is 0.1 s per frame. If we need weaker magnetic field, we need more time for averaging the measured data.

The magnetic field vector component that the magnetic sensor was able to detect simultaneously was only one component among the x-components (H_x) and y-components (H_y), which were parallel to the electrode of the rechargeable battery. As such, to measure two components of H_x and H_y , the magnetic sensor module was rotated

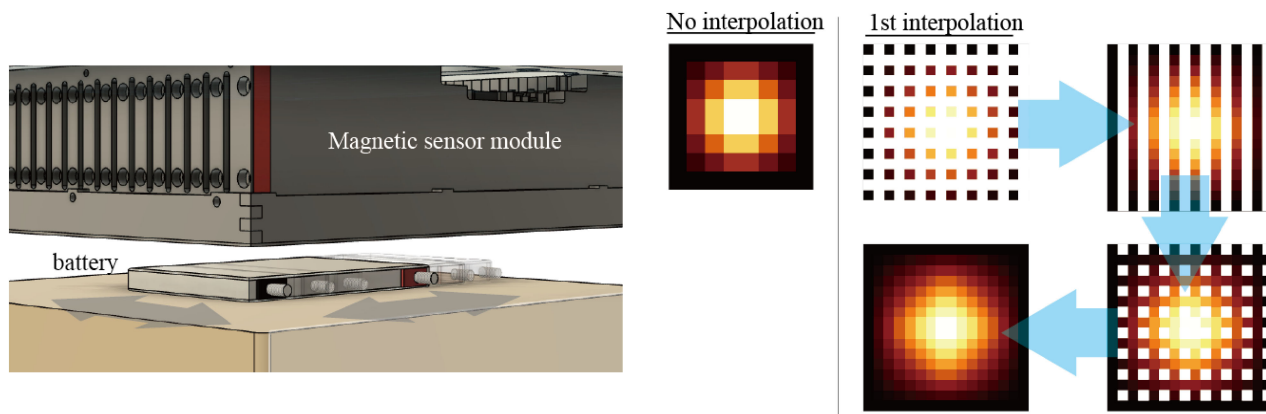


Figure 3. Overview of the interpolation operation. X and Y stage scans bridge the sensor pitch.

90° around the axis perpendicular to the electrode of the rechargeable battery.

The challenge of super high-sensitive magnetic sensing is a magnetic noise originating from something other than the measuring object, such as geomagnetism. A magnetic shield is often used to block this noise. We block magnetic noise by detecting magnetic signal synchronized with frequency of the alternating current applied to the rechargeable battery at all channels. The magnetic signal from the magnetic sensor module was captured in the control PC through a multichannel A/D converter with a sampling rate of 16 bit/10kHz and then detected in the control PC.

The distance between the sample and the magnetic sensor module was determined by having the cell make contact with the magnetic sensor module and then by making it evacuate an arbitrary distance. The contact was detected with a detection sensor installed on the upper part of the sensor module when the Z-stage was moved, while the rechargeable battery was installed to make the sensor module gradually approach the cell. The contact sensor consisted of a spring and a reflective photo-microsensor, as shown in Fig. 2(d). The shaft attached to the sensor module was hung by the spring and detected another shaft that was pushed up by the sensor module and made contact with the rechargeable battery with the photo-micro-sensor.

3.1 Processing of the difference with the reference cell

After spreading from a drawer tab to a collector to an active material, the electric current in the rechargeable battery causes cell reaction at each electrode coordinate (Fig. 4). Generally, the tab is where the electric current concentrates when it is applied because it is often smaller than the electrode. Because the method used for this experiment assumed the measurement target to be the magnetic field that occurs as a result of the electric conductivity distribution, any electric current concentration spot other than the short-circuit point is a factor of disadvantageous for the measurement the short-circuit. Thus, the difference between a reference—the magnetic field distribution image of the rechargeable battery whose electric conductivity distribution in the electrode is spatially uniform—and the magnetic field distribution of the measured cell was processed to nullify the magnetic field caused by the electric conductivity distribution derived from the structure of the cells. This makes it possible to clearly visualize the signal from the abnormal part.

4. Experimental

4.1 Visualization of short-circuited spot of battery cells with large self-discharge

The cell shown in Figs. 5(a) and 5(b) was a laminate cell with an

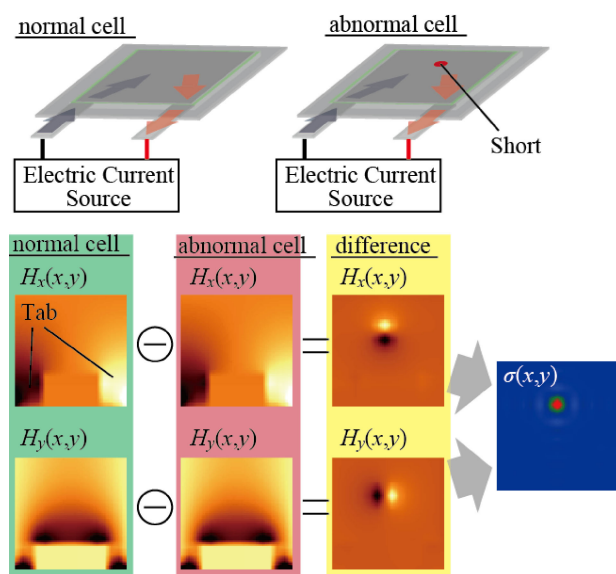


Figure 4. A conceptual diagram of the difference processing. A strong signal is detected in the vicinity of the tab since this is where the electric current concentrates; the signal from the short-circuit point is buried among these. The difference between the magnetic field distribution of a good cell (reference) and that of a broken cell is processed to clearly visualize the breakdown spot.

electrode application area of 74×104 mm and an initial capacity of 170 mAh. The electrode materials of the cathode consisted of 94 % ternary system (NMC), 3 % black acetylene, and 3 % PVDF (those of the anode consisted of 98 % black lead), 1 % CMC, and 1 % SBR. Because there was a separator defects of 12×14 mm in the vicinity of the tab of this cell, the electrodes of the cathode and the anode touched each other, and the battery completely self-discharged from full charge in several seconds. A direct current was applied so that the OCV of the cell could be maintained at 3.3 V, and observation was performed while applying an 80 mAp-p/2 Hz alternating current superimposed on this. The magnetic field distribution was measured for 25 s per frame. These measurement conditions were determined in consideration of shielding and the sensitivity of the magnetic sensor. At this frequency, the impedance phase of the battery is small enough that this system is applicable. The difference between the measured magnetic field distribution and the reference magnetic field distribution was processed, and the internal electric conductivity distribution of the rechargeable battery was visualized based

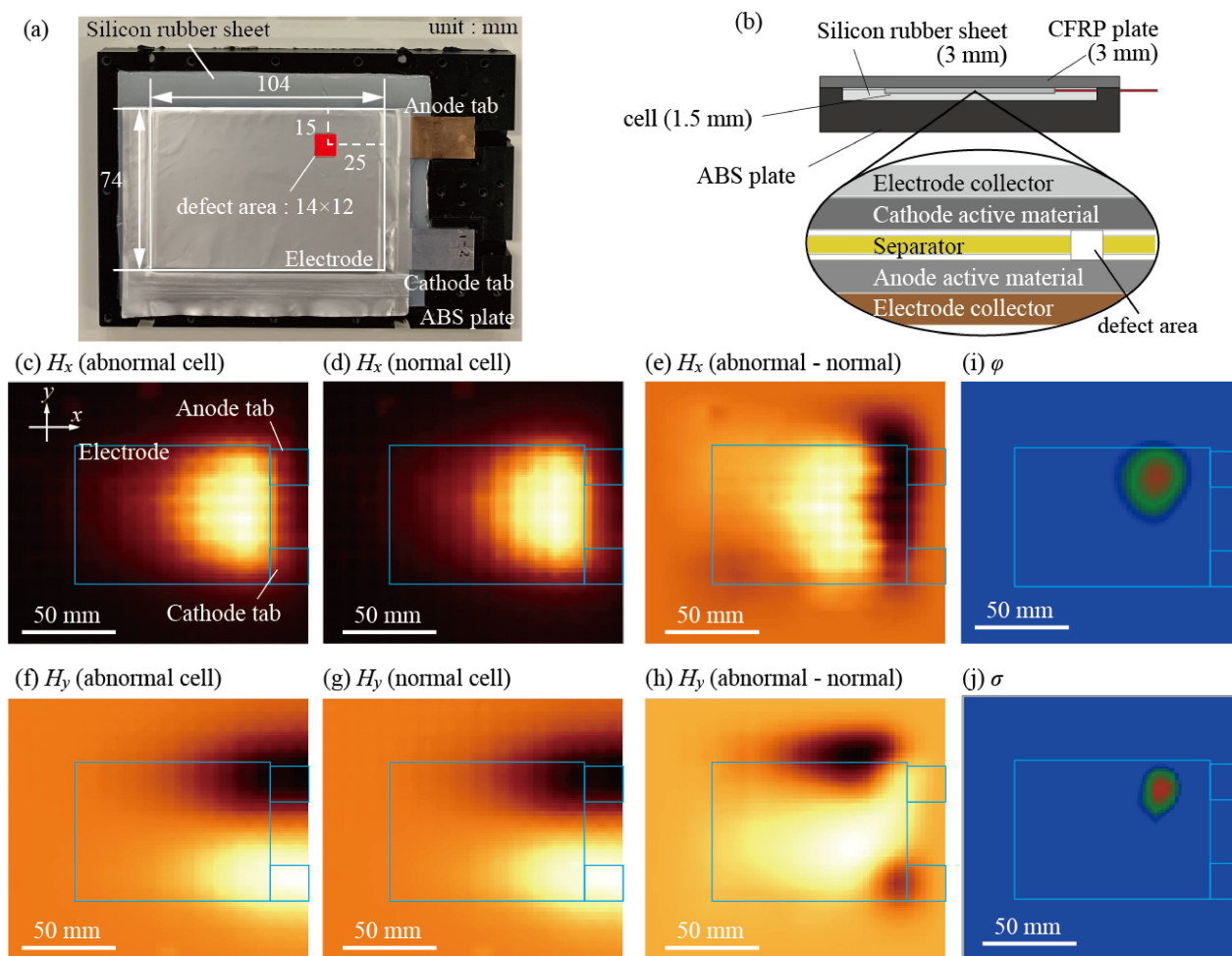


Figure 5. The analysis results of the rechargeable battery cell with a large self-discharge having a separator loss. (a) Dimensions of the cell; (b) inner structure of a clamp jig and the cell; and (c) image of the magnetic field distribution (H_x) of the broken cell obtained by the magnetic imaging system. The electric current enters and exits near the tabs. The electric current is concentrated near each tab, and a strong signal is measured; (d) image of the magnetic field distribution of a normal cell (H_x); (e) image of the difference in the magnetic field distribution between a broken cell and a normal cell (H_x); (f) image of the magnetic field distribution of a broken cell (H_y); (g) image of the magnetic field distribution of a normal cell (H_y); (h) image of the difference in the magnetic field distribution between a broken cell and a normal cell (H_y); (i) Reconstituted potential difference distribution $\varphi(x, y)$ with (e) and (h) as boundary conditions and (j) Reconstituted electric conductivity distribution $\sigma(x, y)$. A spot with high electric conductivity is shown in red, and a strong contrast can be seen in the coordinate corresponding to the spot that lacks the separator.

on the obtained data. Note that, during the measurement, a silicone rubber sheet with the thickness of 3 mm was spread over a plate made of ABS to stabilize the short circuit, and the cell was clamped with a plate made of carbon-fiber reinforced plastic with a thickness of 3 mm. The pressure at this time was 0.1 MPa.

4.2 Change of magnetic field distribution when the cell forming the short circuit

Next, we will show a simulation structure and the result of the measurement of the rechargeable battery cell used to observe the phenomenon that a precipitating metal short circuits between the electrodes. Two sheets of copper measuring 200×150 mm, to which a piece of conductive tape was glued as a tab, are faced parallel and an absorbent sheet with a thickness of 0.13 mm is inserted between these sheets; 1.0 M ($M = \text{mol dm}^{-3}$) copper sulfate aqueous solution (electrolyte) was impregnated in the absorbent sheet [Fig. 6(a)]. When the voltage was applied to this structure, Cu^{2+} in the electrolyte was reduced and precipitated as a metal crystal to short circuits between the electrodes. The structure was electrically insulated by sealing over the copper sheet with an

insulating film made of polyimide with a thickness of 30 μm . This insulation seal included a 22×22 -mm area that lacked insulation, so the electrolyte made contact with only this area. The opposing electrode also lacked the insulation seal within this area; therefore, copper was deposited on the copper sheet only within this uninsulated area. We applied an alternating current of 130 mAp-p/10 Hz to this structure with an overlapping DC current of 64 mA. The maximum value of the generated magnetic field strength is within the range where the magnetic sensor does not overflow. The magnetic field distribution was measured with a measuring range of 240×150 mm, and the multiplication time was set at 0.50 s per frame taking into account the magnetic strength we want to detect. In this experiment, it was necessary to maintain the measurement rate, because the temporal change of the cell was the goal of the observation. Thus, we decided that only the H_x magnetic field needed to be measured. The changes in the magnetic field at each time compared with the magnetic field distribution at the time of the electric current application ($t = 0$ s, immediately after applying current) are shown.

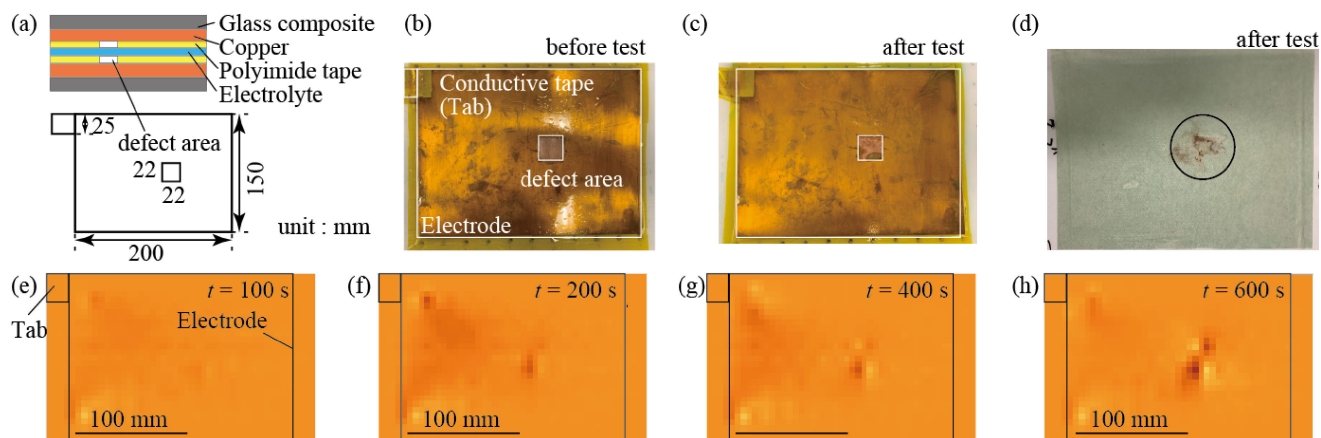


Figure 6. Changes in the images of the magnetic field distribution (H_x) of the cell simulation structure using the electrode with an active site at its center. (a) Sample schematic; (b) photograph of the electrode of cathode before the current application; (c) photograph of the electrode of cathode after the measurement; (d) photograph of the sheet with the electrolyte being impregnated after the measurement; (e)–(h) images of the magnetic field distribution (H_x) when the magnetic field distribution at the current application $t = 0$ (immediately after applying current) is used as a reference. The elapsed time at the time of each image acquisition is (e) 100, (f) 200, (g) 400, and (h) 600 s. It can be seen that, as time passed, the reaction advanced at the separator defect, and the intensity of the magnetic field increased as the electric current increased. Additionally, precipitation was confirmed at the spot that lacked the separator on the sheet with the electrolyte that was impregnated.

5. Result

5.1 Visualization of short-circuited spot of battery cells with large self-discharge

Figures 5(c), 5(d), 5(f), and 5(g) show the magnetic field distribution images of the short-circuit cell and the reference cell. Figure 5(j) shows the electric conductivity distribution obtained based on the images shown in Figs. 5(e) and 5(h). It is difficult to identify the short-circuit point using only the magnetic field distribution of the short-circuit cells (as seen in Figs. 5(c) and 5(f)). However, when the electric conductivity in the rechargeable battery was reconstituted based on the result of the difference processing with the reference, the area with high electric conductivity (in red) can be seen clearly, and the position almost correspond with the separator defect. Figure 5(i) is the reconstructed potential distribution $\varphi(x, y)$. Originally, the gradient should be large near the tab where the current is input and output, but it can be seen that this effect is offset by the difference processing.

5.2 Change of magnetic field distribution when the cell forming the short circuit

Figure 6 shows the appearance of the electrode before and after the current application and the temporal change in the magnetic field distribution obtained by the measurement. Compared with the copper sheet before the electric current was applied, as shown in Fig. 6(b), after the electric current was applied, as shown in Fig. 6(c), the state of the electrode surface changed at the region lacking the insulating tape. Furthermore, it also can be seen that the precipitated copper remained on the electrolyte-impregnated sheet. Figures 6(e)–6(h) show the magnetic variations at the time of current application ($t = 0$ s). There were no changes in the magnetic field distribution at $t = 100$ s, but bright spots began to appear at the center of the images from $\sim t = 200$ s, indicating that the intensity of the magnetic field at this spot increased over time. Based on these results, the magnetic field of the cell changed when the electric current was applied, and the coordinate of the precipitate and the coordinate where the magnetic field distribution image changed corresponded.

6. Conclusions

In this study, we developed a system that performed an in situ measurement of a electric conductivity distribution in a rechargeable battery based on a magnetic field distribution measurement. This system consisted of a sensor module comprising of a two-dimensional array of super high-sensitive magnetic sensors and a calculation process to reconstitute the electric conductivity distribution in the rechargeable battery based on the magnetic field obtained. This sensor module was a 24×24 -ch two-dimensional array of magnetic impedance sensors with a magnetic detection capability of $30 \text{ pT/Hz}^{0.5}$ (at 1 Hz) and a magnetic response frequency of 1 kHz; the magnetic field distribution in the 240×240 -mm range was measured. Additionally, the size of the magnetic reception element was 6 mm, as was the spatial resolution. In this measurement, magnetic noise is blocked including geomagnetism, because it detects the magnetic signal synchronized with frequency of the alternating current applied to the rechargeable battery at all channels. Using this system, we visualized the short-circuit spot in the rechargeable battery where the internal short circuit occurs as a result of the lack of a separator. Additionally, using a rechargeable battery simulation structure, in which the short circuit is formed by the electric current, we observed how the behavior of the magnetic field changed during the electric current application. After the measurement, it was confirmed by opening the structure that the position where metal precipitated corresponded with the position where the magnetic field changed. Since non-magnetic materials are generally used as constituent materials for lithium-ion batteries, the system developed in this study can be applied to various rechargeable batteries, including multi-layer rechargeable batteries, and makes it possible to analyze the effect of a local feature, i.e., the change in the spatial distribution of the electric conductivity, on the characteristics of the entire cell. We expect this to lead to the optimization of the constituents and the conditions of the use of the battery.

Acknowledgments

This work was partially supported by NEDO (New Energy and Industrial Technology Development Organization), SENTAN.JST.

Data Availability Statement

The data that support the findings of this study are openly available under the terms of the designated Creative Commons License in J-STAGE Data at <https://doi.org/10.50892/data.electrochemistry.15175998>.

Correction after Advanced Online Publication

Corrigenda

Since an error was found in the authors' list in all advanced online publication versions including authors' manuscript, uncorrected proof, and corrected proof of this paper published by the authors, it is corrected as follows and correctly shown in the authors' list of this paper under an agreement between ECSJ and all authors.

List of authors and affiliations

(Original)

Seiju MATSUDA,^{a,*§} Shogo SUZUKI,^a Kai YABUMOTO,^a Hideaki OKADA,^a Yuki MIMA,^{b,c} Noriaki KIMURA,^{b,c} and Kenjiro KIMURA^{a,c,d}

^a Graduate School of Science, Kobe University, 1-1 Rokkodai-cho, Nada-ku, Kobe, Hyogo 657-8501, Japan

^b Integral Geometry Science, 1-5-6 Minatojima-minamimachi, Chuo-ku, Kobe, Hyogo 650-0047, Japan

^c New Energy and Industrial Technology Development Organization, 1310 Omiya-cho, Saiwai-ku, Kawasaki, Kanagawa 212-0014, Japan

^d Center for Mathematical and Data Sciences, Kobe University, 1-1 Rokkodai-cho, Nada-ku, Kobe, Hyogo 657-8501, Japan

* Corresponding author: staff-kimuralab@silver.kobe-u.ac.jp

(Corrected)

Seiju MATSUDA,^{a,§} Shogo SUZUKI,^a Kai YABUMOTO,^a Hideaki OKADA,^a Yuki MIMA,^{b,c} Noriaki KIMURA,^{b,c} and Kenjiro KIMURA^{a,c,d,*§§}

^a Graduate School of Science, Kobe University, 1-1 Rokkodai-cho, Nada-ku, Kobe, Hyogo 657-8501, Japan

^b Integral Geometry Science, 1-5-6 Minatojima-minamimachi, Chuo-ku, Kobe, Hyogo 650-0047, Japan

^c New Energy and Industrial Technology Development Organization, 1310 Omiya-cho, Saiwai-ku, Kawasaki, Kanagawa 212-0014,

Japan

^d Center for Mathematical and Data Sciences, Kobe University, 1-1 Rokkodai-cho, Nada-ku, Kobe, Hyogo 657-8501, Japan

* Corresponding author: kimura@gold.kobe-u.ac.jp

The corresponding author apologizes for these errors and any consequent inconvenience to readers.

August 12, 2021

Kenjiro KIMURA

References

1. B. Scrosati and J. Garche, *J. Power Sources*, **195**, 2419 (2010).
2. R. Akolkar, *J. Power Sources*, **232**, 23 (2013).
3. Z. Li, J. Huang, B. Yann Liaw, V. Metzler, and J. Zhang, *J. Power Sources*, **254**, 168 (2014).
4. X. B. Cheng, T. Z. Hou, R. Zhang, H. J. Peng, C. Z. Zhao, J. Q. Huang, and Q. Zhang, *Adv. Mater.*, **28**, 2888 (2016).
5. P. Ping, Q. Wang, P. Huang, K. Li, J. Sun, D. Kong, and C. Chen, *J. Power Sources*, **285**, 80 (2015).
6. U. von Sacken, E. Nodwell, A. Sundler, and J. R. Dahn, *Solid State Ionics*, **69**, 284 (1994).
7. S. Zheng, L. Wang, X. Feng, and X. He, *J. Power Sources*, **378**, 527 (2018).
8. K. Nishikawa, T. Mori, T. Nishida, Y. Fukunaka, and M. Rosso, *J. Electroanal. Chem.*, **661**, 84 (2011).
9. I. W. Seong, C. H. Hong, B. K. Kim, and W. Y. Yoon, *J. Power Sources*, **178**, 769 (2008).
10. W. Zhao, G. Luo, and C. Y. Wang, *J. Electrochem. Soc.*, **162**, A207 (2015).
11. R. Zhao, J. Liu, and J. Gu, *Energy*, **123**, 392 (2017).
12. B. Mao, H. Chen, Z. Cui, T. Wu, and Q. Wang, *Int. J. Heat Mass Transfer*, **122**, 1103 (2018).
13. X. Feng, J. Sun, M. Ouyang, F. Wang, X. He, L. Lu, and H. Peng, *J. Power Sources*, **275**, 261 (2015).
14. I. Uchida, H. Ishikawa, M. Mohamedi, and M. Umeda, *J. Power Sources*, **119–121**, 821 (2003).
15. K. C. Chiu, C. H. Lin, S. F. Yeh, Y. H. Lin, and K. C. Chen, *J. Power Sources*, **251**, 254 (2014).
16. J. Wang, W. Mei, Z. Cui, W. Shen, Q. Duan, Y. Jin, J. Nie, Y. Tian, Q. Wang, and J. Sun, *Appl. Therm. Eng.*, **171**, 115082 (2020).
17. T. Yokoshima, D. Mukoyama, F. Maeda, T. Osaka, K. Takazawa, S. Egusa, S. Naoi, S. Ishikura, and K. Yamamoto, *J. Power Sources*, **393**, 67 (2018).
18. J. Lamb and C. J. Orendorff, *J. Power Sources*, **247**, 189 (2014).
19. Y. Mima, N. Oyabu, T. Inao, N. Kimura, and K. Kimura, *Proceedings of IEEE CPMT Symposium Japan*, **257** (2013).
20. K. Kimura, Y. Mima, and N. Kimura, *Subsurface Imaging Science & Technology*, **1**, 16 (2017).
21. T. Uchiyama, K. Mohri, Y. Honkura, and L. V. Panina, *IEEE Trans. Magn.*, **48**, 3833 (2012).